Thermophoretically driven water droplets on graphene and boron nitride surfaces

Rajegowda, Rakesh; Kannam, Sridhar Kumar; Hartkamp, Remco; Sathian, Sarith P.

DOI
10.1088/1361-6528/aab3a3

Publication date
2018

Document Version
Final published version

Published in
Nanotechnology

PAPER

Thermophoretically driven water droplets on graphene and boron nitride surfaces

To cite this article: Rakesh Rajegowda *et al* 2018 *Nanotechnology* **29** 215401

IOP Publishing Nanotechnology
Nanotechnology 29 (2018) 215401 (11pp) https://doi.org/10.1088/1361-6528/aab3a3

Thermophoretically driven water droplets on graphene and boron nitride surfaces

Rakesh Rajegowda[1], Sridhar Kumar Kannam[2,3], Remco Hartkamp[4] and Sarith P Sathian[1,5]

[1] Department of Applied Mechanics, Indian Institute of Technology Madras, Chennai 600036, India
[2] Faculty of Science, Engineering and Technology, Swinburne University of Technology, Melbourne, Victoria 3122, Australia
[3] School of Sciences, RMIT University, Melbourne, Victoria 3001, Australia
[4] Process and Energy Department, Delft University of Technology, Leeghwaterstraat 39, 2628 CB Delft, Netherlands

E-mail: r.rakzz@gmail.com, urssrisri@gmail.com, remcohartkamp@gmail.com and sarith@iitm.ac.in

Received 16 December 2017, revised 19 February 2018
Accepted for publication 2 March 2018
Published 27 March 2018

Abstract

We investigate thermally driven water droplet transport on graphene and hexagonal boron nitride (*h*-BN) surfaces using molecular dynamics simulations. The two surfaces considered here have different wettabilities with a significant difference in the mode of droplet transport. The water droplet travels along a straighter path on the *h*-BN sheet than on graphene. The *h*-BN surface produced a higher driving force on the droplet than the graphene surface. The water droplet is found to move faster on *h*-BN surface compared to graphene surface. The instantaneous contact angle was monitored as a measure of droplet deformation during thermal transport. The characteristics of the droplet motion on both surfaces is determined through the moment scaling spectrum. The water droplet on *h*-BN surface showed the attributes of the super-diffusive process, whereas it was sub-diffusive on the graphene surface.

Keywords: thermophoresis, water, graphene, boron nitride, nanotransport

(Some figures may appear in colour only in the online journal)

1. Introduction

The field of nanofluidics has seen a dramatic growth in recent years owing to countless innovative methods and applications. From water desalination [1] to electronic cooling processes [2], there is an explosive growth in the fields of material manipulation and transportation at the nano-scale. Despite technological advances, it remains challenging to gain molecular-level insight into fluid and particle transport. Accurate mechanical transport in nanochannels requires detailed knowledge of slip behavior, and relatively large forces are needed to cause significant flow rates [3]. Alternatively, a fluid and particle transport can also be driven by the forces generated from an electric field, thermal gradient or chemical potential. Whereas, thermodiffusion is considered to produce high drifting forces for the mass transportation at a nano-scale [4] and it allows the micro-scale manipulation of small particles and molecules [5–9]. The physics involved in diffusion driven by a thermal gradient is known as thermophoresis (Soret effect) [10]. Thermophoresis is a phenomenon where the driving force is a gradient in the phonon distribution along the direction of the thermal gradient [11]. Also, thermophoresis is considered to be the important cause of molecular traps in hydrothermal vents (rock pores), which eventually led to the origin of life [12].

In previous reports, interaction energy has been discussed in connection with the thermophoretic mechanism and used to calculate thermophoretic force [13, 14]. The potential energy and thermophoretic forces acting on the transported fluid or solid object varied linearly with the applied thermal gradients [9, 13, 14]. In general, for a smaller power consumption, a high driving force is generated during thermophoresis, when compared to mechanical methods. A thermal gradient as low as $0.18\,\mathrm{K\,nm^{-1}}$ is sufficient to overcome the friction and to trigger the movement of water droplets from one end to the other end of a carbon nanotube [13]. When water is confined

[5] Author to whom any correspondence should be addressed.

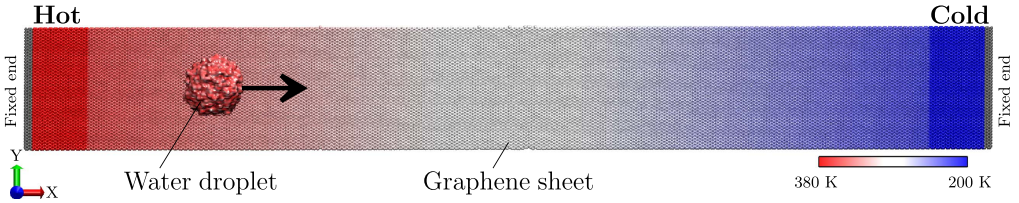

Figure 1. The computation set-up of water–graphene system. The hot and cold zone is represented by the red and blue colors representing the gradient in temperature (2.5 K nm^{-1}).

in a nanochannel, the interaction between water and confining walls causes the deviation of the confined water properties from its bulk water values [15, 16]. For example, the viscosity and phase transition temperature are affected [17]. The difference in water properties is ascribed to hydrogen bonds between water molecules, potential energy of interaction and potentially the curvature of the nano-channels [18]. The flow properties of water confined in nano-channels are representative of flow through aquaporins [19], which play a critical role in controlling the water content of the cells. Most prior studies [11, 20–24] on thermophoresis have focused on one-dimensional motion, for example through a carbon nanotube. Very recently, there have been efforts to consider the transport of solids on two-dimensional surfaces employing thermal forces. Thermophoretic transport of a fullerene [25], carbon nanotube [25] and graphene nanoflakes [26] over a graphene sheet was successful, and nano-cargoes were observed to diffuse against the thermal gradient in a fluctuating path. The natural sliding of graphene nano-flakes over a long graphene ribbon was observed even at shallow thermal gradients [26]. The motion of nano-flakes is possible even at low thermal gradients due to the weak interactions with the graphene ribbon and similar effects are expected on molybdenum disulfide and hexagonal boron nitride (*h*-BN) surfaces [27]. Understanding the transport behavior of fluid while interacting with these materials is important for wide-ranging applications. For example, in the pumping of fluids into nano-channels for conducting experiments, the waste heat management, targeted cooling in nano-electronic systems and many other applications. While thermophoretic transport of small solid objects on a surface has received recent attention [25, 26], no study of thermophoretic transport of fluid on a surface has yet been conducted to our knowledge.

In the present study, a water nano-droplet is transported along graphene and *h*-BN nano-ribbons by applying a thermal gradient to the substrate. Non-equilibrium molecular dynamics simulations are employed to determine the effect that a thermal gradient applied to the substrate has on the transport of a water droplet. To obtain insight into the movement and deformation of a droplet, the instantaneous contact angle of the water droplet was monitored during the thermal transport. With this study, we aim to understand thermophoretic transport of a water droplet on a two-dimensional surface. We also investigate the direct effect of surface wettability and dynamic contact angle on water droplet transport under a thermal gradient, which has not been investigated previously. The present study contributes to an improved understanding of the nano-droplet transport on a surface, which is necessary to develop novel methods of nano-transportation and nano-electronic heat management systems. In the next section, the simulation details are discussed. The results obtained by varying magnitude of the thermal gradient acting on water droplet over the graphene and *h*-BN sheets are analyzed and presented in the results section.

2. Methodology

Graphene and *h*-BN sheets were simulated independently as substrates with a single atom thickness to study the transport of water nano-droplet. Both sheets are 80 nm long and 10 nm wide and the height of simulation box is 20 nm. Periodic boundary conditions were applied in all directions. Along the length, both the edges were kept rigid for 0.5 nm to prevent drifting and bending of the sheets. The same simulation conditions are applied to both the systems. The temperature of the sheet up to a length of 3.5 nm from the fixed ends is controlled through Nosé-Hoover thermostat to maintain the hot and cold ends, respectively, while the rest of the sheet is kept at a constant energy (i.e. microcanonical ensemble). We have considered 1200 water molecules as a droplet to study the transport from one end of the sheet to the other. First, the water droplet is equilibrated for 1.5 ns and its center-of-mass is constrained at the hot end of the sheet during equilibration. Further, the sheet is equilibrated until a temperature gradient develops along the length of the sheet. The water droplet is unconstrained during the production run to undergo thermophoresis. Then, thermophoresis is investigated for various thermal gradients from 0.5 to 2.5 K nm^{-1} for every 0.5 K nm^{-1} intervals with the maximum temperature at the hot end being 380 K and a cold end temperature of 200 K. The center-of-mass position is recorded until the droplet reaches the cold end. The water–graphene simulation system is shown in figure 1, with the color of the sheet representing the gradient in temperature. Figure 2 shows a cropped top and side view of the water droplet for the water–graphene and water–*h*-BN systems. The graphene sheet did not undergo any deformation when heated. Whereas, the *h*-BN sheet is found to undergo thermal expansion when heated [28]. Hence, the *h*-BN sheet is allowed to expand along its length during the equilibration, after which it ends are fixed. The *h*-BN sheet at 2.5 K nm^{-1} expanded by 20% of its original length. As the flexible substrates are used to transport the droplet, it is important to avoid unwanted deformation modes due to internal stresses during the transport of the droplet.

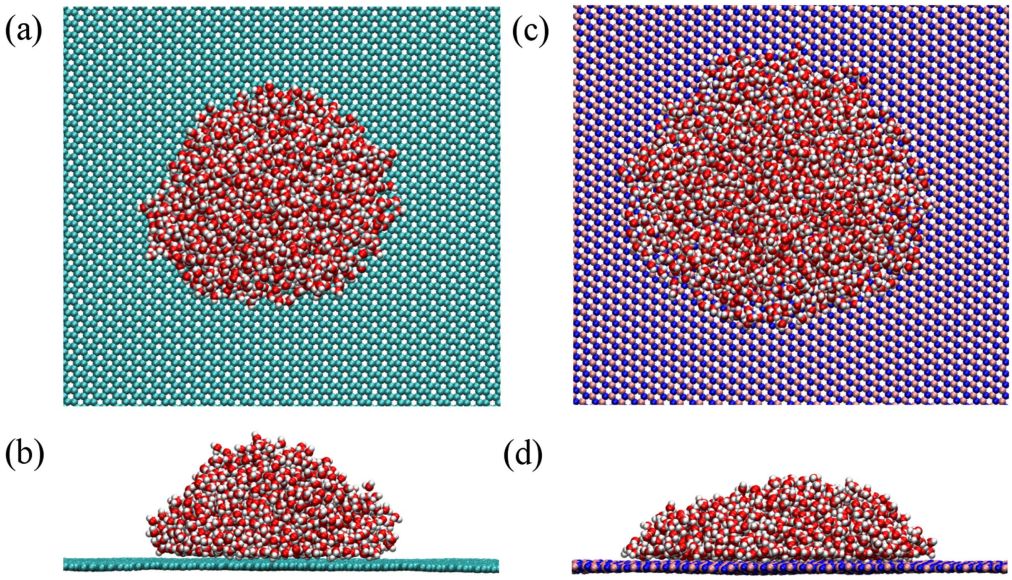

Figure 2. A cropped top (a), (c) and side (b), (d) view of a water droplet on a substrate. The substrate in (a), (b) is graphene and (c), (d) is *h*-BN. Oxygen, hydrogen, carbon, boron and nitrogen atoms are represented by red, white, cyan, pink and purple colored spheres, respectively.

The simulations are conducted using the LAMMPS [29] package. Each simulation is run with a time-step of 1 fs. Water is modeled with the SPC/E [30] model, with the rigid molecular structure enforced via the SHAKE algorithm. The non-bonded interactions (except carbon–carbon) are based on the CHARMM force field [31] with a cut-off radius of 12 Å (inner) and 14 Å (outer). The shifting functions are used to ramp the non-bonded interaction energy and force values smoothly to zero beyond the cut-off. Carbon interactions in the graphene ribbon are represented by the REBO potential [32]. The Tersoff potential [33] is used to define the inter-atomic potential of the *h*-BN ribbon. The Lorentz−Berthelot mixing rule is used to model interactions between the atoms of different types.

3. Results and discussions

3.1. Effect of surface wettability

Figure 2 shows a water droplet on surfaces with varying wettability, where (a) and (b) show the top and side view of a water droplet on a graphene sheet, whereas (c) and (d) show the top and side view of a water droplet on an *h*-BN sheet. The wetting observed in the simulation snapshots suggest that graphene is more hydrophobic than *h*-BN, which is consistent with the work of Li and Zeng [34]. The shape of the droplet on the graphene sheet is hemispherical, while it is almost flat on the *h*-BN surface. The random movement of the water droplet is greater on the graphene than on the *h*-BN surface. The equilibrium MD simulations are performed for 20 ns to calculate the number density contours (figure 3). The volume of the simulation box is divided into cubical bins with sides of 0.01 nm. The center-of-mass axis along the *z*-direction of the water droplet is used as the reference origin for contour plotting. The contour plots give an averaged droplet profile that can be used for measuring contact angles. The contact angle of a droplet is often calculated from the slope of an elliptical fit where it intercepts the solid surface ($z_u = 0$). However, the contact angle for a water–graphene system reported in previous studies is inconsistent, mainly due to the different assumptions made about the shape of the droplet [35–37]. From figure 3 it is evident that the contour profile has a dense region at the base of the droplet, due to the formation of a hydration layer, with a thickness of 0.4 nm. The hydration layer thickness is considered as the critical distance (z_c), below which the data is excluded from curve fitting and contact angle measurements. The consideration of z_c plays a vital role, as the contact angle is estimated from extrapolating a fitted curve from z_c until the surface of substrate. Consequently, the value of z_c and the functional form of the fit can affect the resulting contact angle.

The elliptical and polynomial functions are used to fit the isodensity points to identify the best fit of the data as considered in the previous reports [36, 37]. Figure 4(a) shows an elliptical (equation (1)) and polynomial (third order) fit of the isodensity points obtained from the outermost line of figure 3(a). The radius of the elliptical equation is given by

$$r(z) = a + b\sqrt{c^2 - z^2}, \qquad (1)$$

where a, b and c are constants, and elliptical radius r is a function of z. Fitting the data to the water-graphene system gives the contact angles of 86.1° and 77.5° for an elliptical and polynomial fit, respectively. The uncertainty in the contact angle determined by the elliptical and polynomial functions are close to 9°. Though the angle obtained from an elliptical fit matches the water–graphene literature [35] more accurately, the polynomial fit gives a better extrapolation of the data points. Henceforth, the polynomial function is used for fitting the isochoric profiles as per the reasoning of

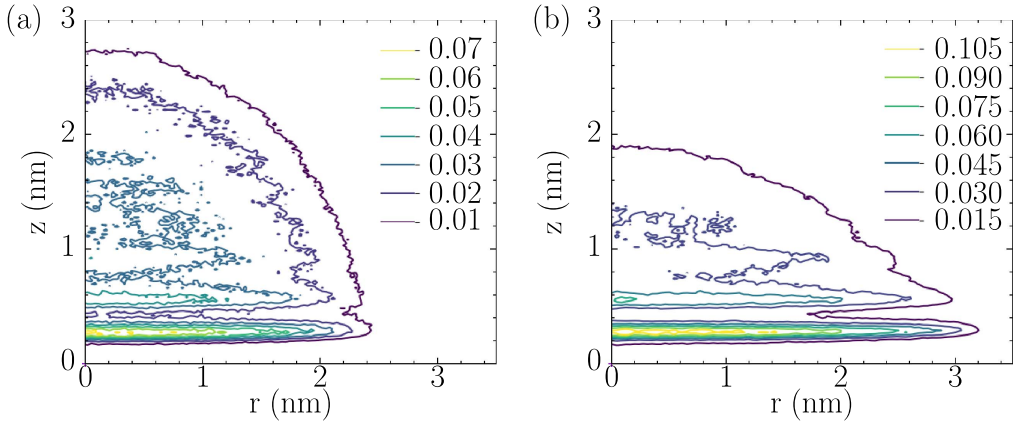

Figure 3. The number density contours are based on the number of water molecules in each bin on (a) graphene and (b) *h*-BN sheets. Average number of atoms per cubical bin of side 0.01 nm is represented in labels.

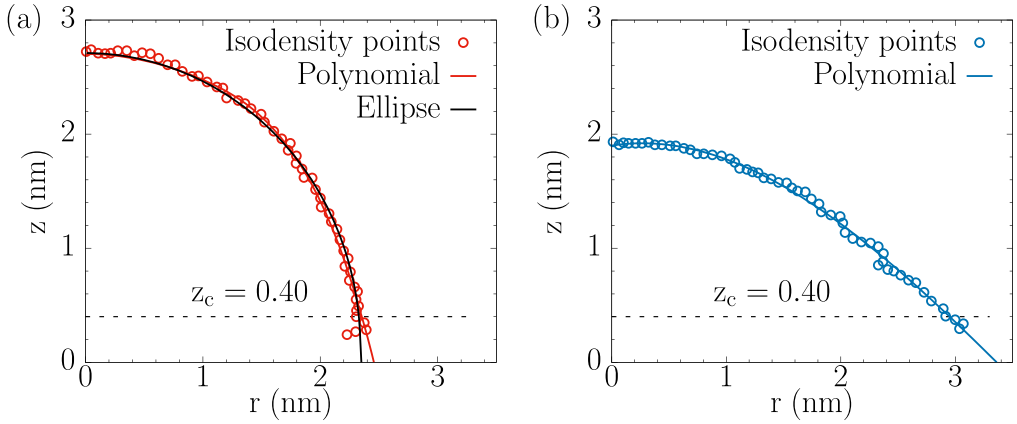

Figure 4. Fitting of the outer isodensity line, taken from the contour plot in figure 3 for (a) graphene and (b) *h*-BN systems. For a graphene system, both elliptical and third order polynomial fit is done to compare the difference in the estimation of contact angle.

Giovambattista *et al* [38] that no geometrical assumption is needed. Also, there are methods to measure contact angle by considering only the center-of-mass and radius of the droplet [39] without depending on the droplet profiles. Similarly, figure 4(b) shows a polynomial fit of the isodensity points obtained from the outermost line of figure 3(b) for a water–*h*-BN system. An average contact angle of 44.5° is measured, in agreement with previous experimental and simulation reports [40]. The difference in contact angle with respect to that on graphene indicates that graphene is considerably more hydrophobic than *h*-BN [35, 40]. Thus, the notable difference in wettability of the two surfaces suggests different dominance in modes of transport on these surfaces.

One-dimensional binning perpendicular to the surface is done to measure the number of water molecules as a function of the distance from the sheet. The binning procedure is similar to that followed for the contours to get the isochoric lines. Figure 5 shows the number of water molecules distributed normal to the surface. A dense water layer is found close to the surface, within a distance of $z \approx 0.4$ nm for both systems. Oscillations in the first and second hydration layers reflect a high degree of spatial ordering of water molecules in this region. At larger distances from the surface, the number of water molecules gradually decrease to zero for both of the

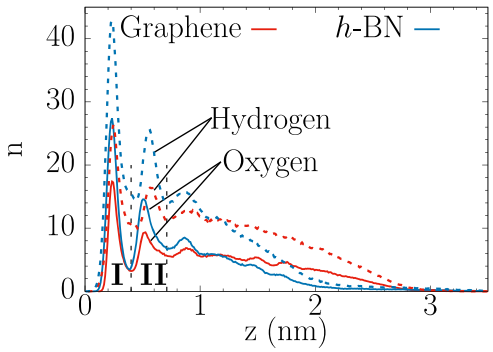

Figure 5. The variation of the number of water molecules normal to the surface, through the center of mass of the droplet for graphene and *h*-BN sheets. Dotted lines indicate the first and second hydration layer of the droplet.

systems, which is a typical indication of a random isotropic distribution of the molecules. The water droplet has spread more on the *h*-BN surface.

3.2. Effect of thermal gradient on nanodroplet

Moving a droplet over a surface requires sufficient driving force to overcome the surface friction barrier due to adhesion

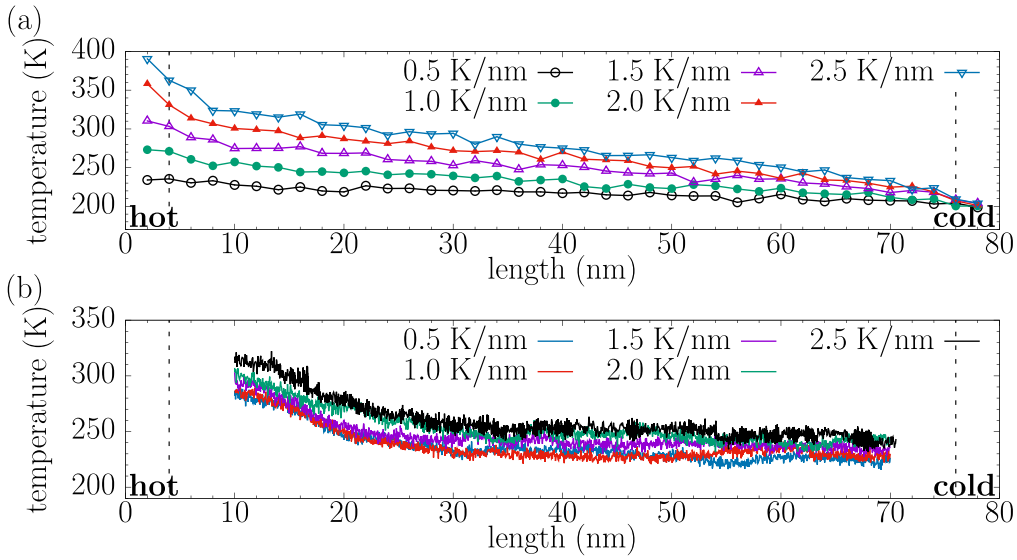

Figure 6. The temperature of (a) a graphene sheet along its length and (b) water droplet as it is transported over a graphene sheet at various thermal gradients.

forces. In a previous study [26], a nanoflake is thermophoretically transported along a graphene sheet, where a thermal gradient developed a potential energy gradient along the graphene sheet that helped the nanoflake to overcome the friction barrier. Interestingly, there are no equivalent studies concerning the transport of liquid droplets under thermophoresis. We have carried out non-equilibrium MD simulations for five thermal gradients from 0.5 to 2.5 K nm^{-1} at an interval of 0.5 K nm^{-1}, on graphene and *h*-BN surfaces. The maximum temperature at the hot end is 380 K and the cold end temperature is 200 K. The maximum temperature is raised until 380 K, above which the water droplet starts evaporating. The freezing temperature of the SPC/E water model is around 215 K [41]. Although the cold end of the surface has a temperature below the freezing temperature of SPC/E water, the droplet remains in the liquid phase. The temperature of the water droplet remains close to 230 K at 0.5 K nm^{-1} and 265 K at 2.5 K nm^{-1} even after reaching the cold end of the graphene sheet. The water droplet temperature does not reach the lowest substrate temperature over the short time, during the droplet transport. In reality, the temperature range of liquid water is limited from 273–373 K. The narrow temperature window, and possibly larger substrate length poses a limitation on the attainable thermal gradient. The usage of ionic liquids could be the possible alternative for energy and heat transfer applications, as ionic liquids remain in a liquid state for a wide temperature range, and are non-flammable and nonvolatile [14].

Figure 6(a) shows the temperature profile along the length of the graphene sheet, measured in bins of 0.2 nm. The nonlinear temperature profile indicates a non-Fourier heat conduction, consistent with the literature [8, 13, 23, 24]. The hot end temperature of the graphene sheet is thermostated at 380 K (the highest temperature used in our study), which is above the boiling temperature of water. However, during every simulation, the water droplet is introduced and equilibrated 6 nm away from the hot zone of the sheet, where the graphene sheet temperature is approx 330 K for a thermal gradient of 2.5 K nm^{-1}. Figure 6(b) shows the evolution of the water droplet temperature as it is transported along the length of the sheet. For the temperature gradient of 2.5 K nm^{-1}, the temperature of the water droplet never reached a value above 320 K during the simulations and the temperature is reduced to 265 K as droplet is transported to the colder end of the sheet. Hence, no evaporation occurs. The change in the temperature gradient of the sheet has a direct effect on the water droplet, as the droplet temperature get raised to 320 K at 2.5 K nm^{-1} and reduced to 286 K at 0.5 K nm^{-1} from its equilibration temperature of 300 K during the initial stage of the production run.

Figures 7(a) and (b) show the trajectory of the water droplet on the graphene and *h*-BN surfaces, respectively, for the case of 2.5 K nm^{-1}. As the graphene is less hydrophilic in comparison to the *h*-BN sheet, the graphene surface offers low resistance and provide less adhesion force for the droplet transport. The trajectories indicate that the water droplet has the freedom to roam around and crosses the periodic boundary multiple times on the graphene sheet, whereas steady displacement of the droplet is observed on the *h*-BN sheet. Consequently, the droplet travels a larger distance on the graphene sheet than on *h*-BN, while the streaming motion is in fact faster on the *h*-BN sheet. The evolution of center-of-mass of the droplet along the length of the graphene and *h*-BN sheets are plotted in figures 8(a) and (b), respectively for various thermal gradients. The data shown are the average of five individual simulations for various seed values. The droplet reaches the cold end of the sheet quicker as the temperature gradient is increased in both the systems. The average time needed for the water droplet to move from hot end to cold end for both graphene and *h*-BN systems are tabulated in table 1. Thus, *h*-BN can be more suitable than graphene to facilitate fast and stable thermal transport of water nanodroplets. From preliminary trajectory analysis, the random path taken by the droplet on graphene reduces the resultant velocity of droplet along the length

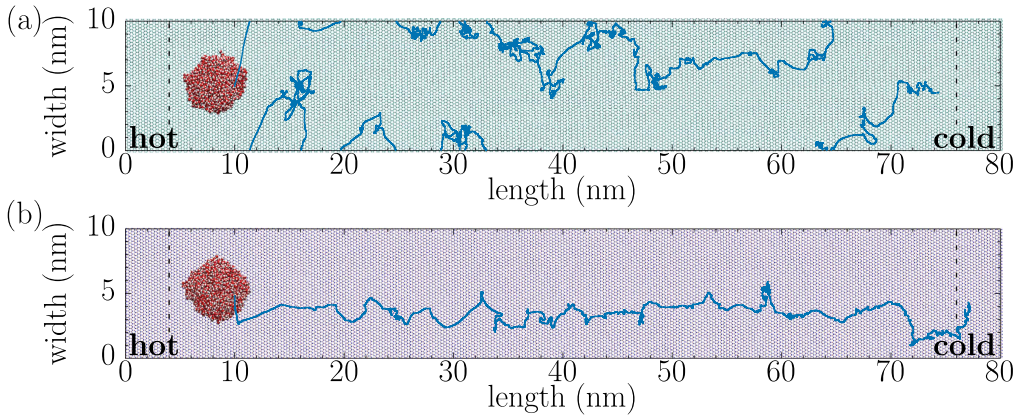

Figure 7. The trajectories of the water droplet on the (a) graphene and (b) *h*-BN sheets at 2.5 K nm^{-1}.

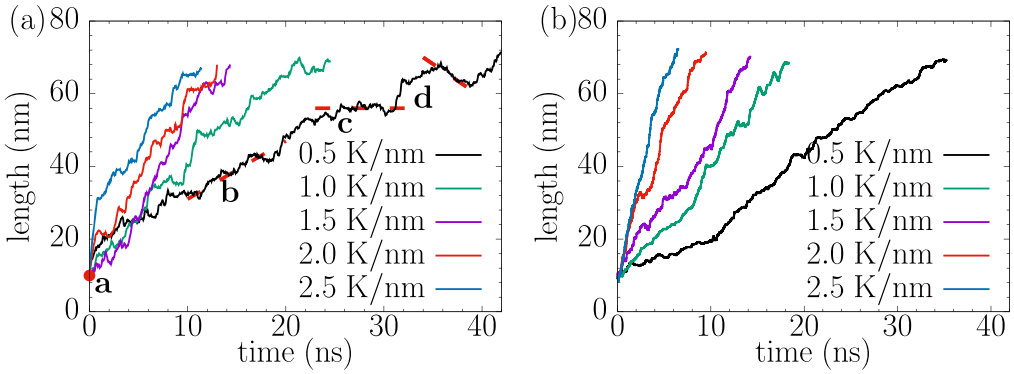

Figure 8. Position of the center-of-mass of nano-droplet on (a) graphene and (b) *h*-BN sheet as a function of time for the various thermal gradients. The point a and dashed line (b, c and d) represents the initial/equilibrium state, forward movement, stagnant state and backward movement of the water droplet, respectively.

Table 1. The average time taken by the water droplet to travel from the hot to cold end of the sheet.

Temperature gradient (K nm^{-1})	Time (ns)	
	Water–graphene	Water–*h*-BN
0.5	42.35	35.43
1.0	21.68	18.35
1.5	14.45	14.17
2.0	12.82	9.41
2.5	10.78	6.56

of the sheet. The water droplet movement on the graphene surface is not in the straight line and has been observed to move erratically, whereas the same is not observed on the *h*-BN surface (figures 7(a) and (b)). Also, from table 1, the time taken by the water droplet to travel from the hot to the cold end of the sheet on the *h*-BN surface is less in comparison to graphene. Thus the *h*-BN sheet can be considered as a suitable candidate for targeted droplet transport in heat management applications. This is further investigated via diffusion analysis.

To confirm that thermophoresis drives the motion of the water droplet, we have calculated the thermophoretic forces acting on the droplet. Figures 9(a) and (b) show, respectively, the center-of-mass velocity (v_{cm}) and the tangential force acting on the droplet along the length of sheet as a function of time, at a thermal gradient of 2.5 K nm^{-1} for the water-graphene system. The velocity and driving force value for the initial 1 ns is considered for energetic and thermophoretic force analysis (see figures 9(a) and (b) inset, respectively). Though the thermal gradient is imposed only along the length of the sheet, there is no necessity of having unidirectional transport as reported for carbon nanotubes [13, 14]. The mean force due to thermal noise is negligible but it created imbalance, which causes the droplet to oscillate. From the velocity profile it is evident that the droplet received a very high initial acceleration due to the applied thermal gradient. The sudden experience of thermal gradient on the droplet could lead to instant change of momentum, leading to higher initial acceleration. As the hot end temperature is reduced, the initial velocity of the droplet is also observed to decrease significantly for both graphene and *h*-BN systems. The insets in figures 9(a) and (b) show that maximum force of 10 pN acts on the droplet, causing the droplet to reach a velocity of nearly 40 m s^{-1}, after which the driving force and velocity decrease. The velocity data show no particular trend, in contrast to the thermophoretic velocity of a droplet in a carbon nanotube [13, 14], for which periods of acceleration, steady flow, and deceleration were identified. Thus, we used figure 8, the evolution of the center-of-mass with time to represent the different phases of transport at 0.5 K nm^{-1}. The static position is represented by point a and the dashed lines

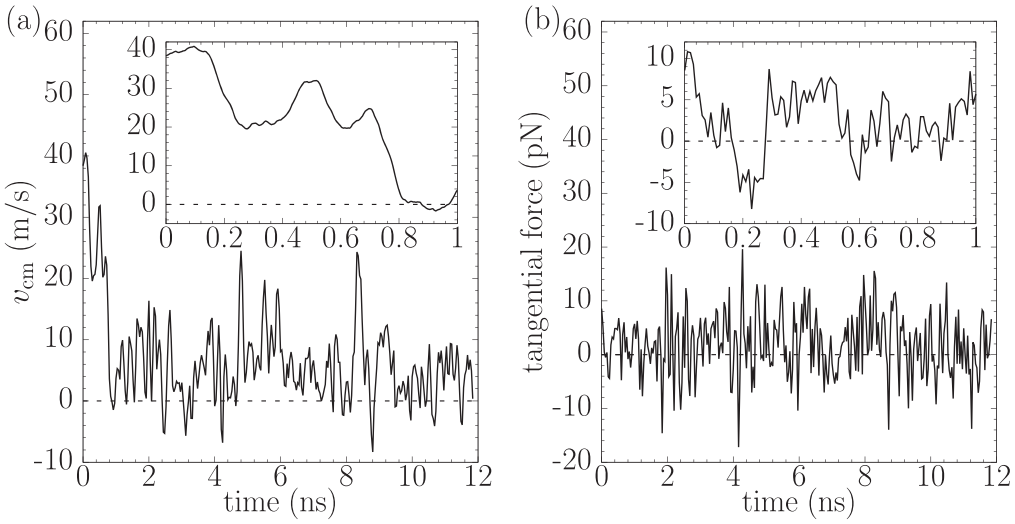

Figure 9. Change in (a) the longitudinal velocity of the water droplet center-of-mass and (b) the tangential force acting on the droplet over time along the length of the graphene sheet at 2.5 K nm^{-1}. The velocity and force value for initial 1 ns is considered for energetic and thermophoretic force analysis.

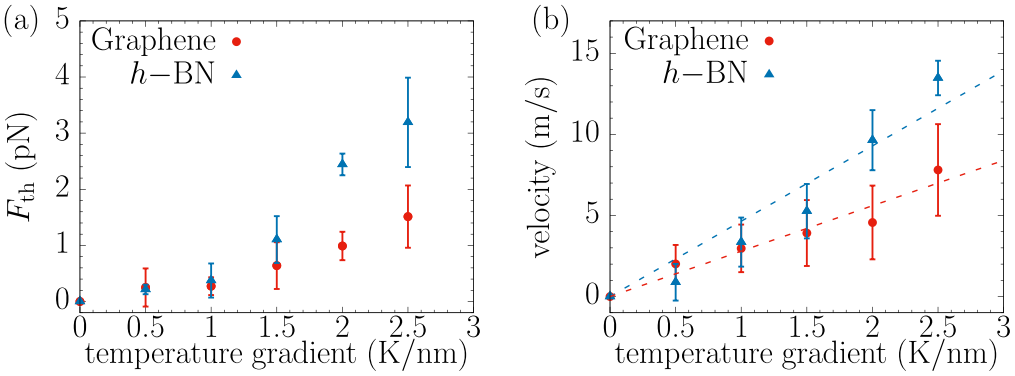

Figure 10. (a) The thermophoretic forces and (b) the average velocity of the water droplet for various thermal gradients along the length of graphene and *h*-BN sheets. Filled points denote results calculated from the initial 1 ns in the non-equilibrium simulations, error bars denote the standard error calculated from five individual simulations. Dashed line denotes the linear fit of the calculated results.

labeled b, c and d show the acceleration, steady/neutral and deceleration phases, respectively.

We have considered only the average initial driving force acting along the length of the sheet obtained from the production run (inset of figure 9(b)) for the calculation of the thermal driving force [13]. Figure 10(a) shows that the thermophoretic driving force increases nonlinearly with the imposed thermal gradient. Earlier studies [13, 14] on water–carbon nanotube systems have reported a linear variation of the thermophoretic driving force against the applied thermal gradient. The water droplet was driven in a carbon nanotube by a thermal gradient varying from 0.18–1.48 K nm^{-1}. Similarly, the thermal gradient varying from 0.5–2.5 K nm^{-1} is used in the present study. The graphene and *h*-BN system generated a thermophoretic force of 1.51 pN and 3.19 pN forces, respectively at a thermal gradient of 2.5 K nm^{-1}. Figure 10(b) shows that the average velocity of the droplet is in linear relation with the applied thermal gradient which is consistent with the previous reports [11, 13, 14]. When the amount of water molecules in the droplet is increased, the average velocity and thermophoretic force acting on the droplets are found to be decreased. However, no appreciable change in the contact angle is observed for the various sizes of the water droplet considered in our study. Figures 11(a) and (b) shows the variation of the thermophoretic force and average velocity of droplet as a function of the droplet size on graphene surface, respectively. It is observed that the thermophoretic force acting on the droplet and the average velocity of the droplet decrease linearly with an increase in the size of water droplet at a thermal gradient of 2.5 K nm^{-1}.

The interfacial friction coefficient (λ) at the droplet-surface interface is investigated to address the difference in driving force acting on the water droplet due to graphene and *h*-BN surfaces. The interfacial friction coefficient is calculated by the ratio of tangential force (F) per unit surface area (A) and slip velocity (v_{slip}) [42], given by

$$\lambda = \frac{F}{Av_{slip}}. \tag{2}$$

The average tangential force exerted by the water droplet on the graphene surface is calculated from the data shown in figure 9(b). The droplet-surface contact area of water–graphene

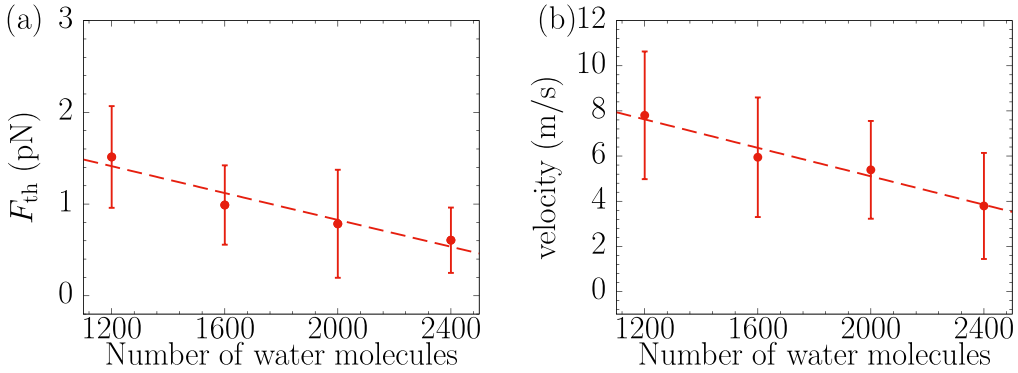

Figure 11. (a) Variation of the thermophoretic force acting on the droplet with droplet size and (b) the average velocity of droplet as a function of the droplet size on graphene surface, at the thermal gradient of 2.5 K nm^{-1}. The dashed lines indicate a linear fit of the data.

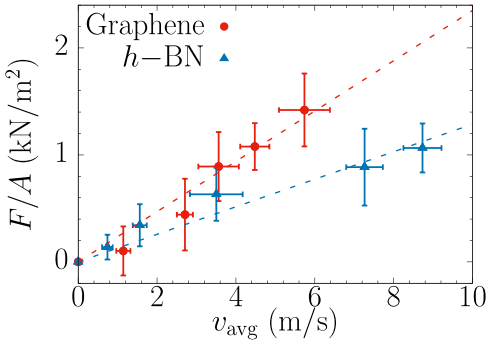

Figure 12. The tangential force exerted on the graphene and *h*-BN sheets per unit area against the average velocity of the water droplet. Error bars in both *x* and *y* directions denote the standard errors calculated from five individual simulations. Friction coefficient is the slope of the linear fit, denoted by dashed lines.

and water–*h*-BN systems are 15.91 and 28.31 nm^2, respectively. The average droplet velocity close to the surface is taken as a slip velocity, which is measured from the simulations for various thermal gradients. Figure 12 shows the tangential force per unit area against the average velocity for graphene and *h*-BN surfaces. The frictional coefficient is calculated as the slope of tangential force and the average velocity of the water droplet. As the tangential force is varying linearly with the average velocity, the frictional velocity is considered to be independent of the droplet transport. The friction coefficient of water–graphene and water–*h*-BN surfaces are calculated as 235.4 and 128.7 Ns m^{-3}, respectively. The friction coefficient of the water–graphene system is nearly twice as high as the friction coefficient of the water–*h*-BN system, this may be the cause of the time delay in the transport of the water droplet on the graphene sheet.

The droplet was found to undergo deformation while moving under the thermal gradient. The advancing and receding angles are identified based on the direction of the droplet motion. Figures 13(a)–(d) show snapshots of the droplet in an initial/equilibrium state, forward movement, stagnant state and backward movement when submitted to a thermal gradient of 0.5 K nm^{-1}. The corresponding simulation time of each condition is already indicated in figure 8. It was not possible to predict the dynamic contact angle of the water droplet by taking a time average or by averaging over various simulations. The dynamic contact angle is therefore calculated from the respective number density contour plot. A two-step procedure is followed to calculate the advancing (θ) and receding (ϕ) contact angles. First, the outer most isochoric contour line is chosen, and isodensity points are extracted. Second, the isodensity points are fitted with a third order polynomial to obtain a droplet profile. The advancing and receding contact angles are then measured by drawing a tangent to the fit. The difference between the two angles measured represents the contact angle hysteresis ($H = \theta - \phi$). Figure 13(e) shows the droplet profile for the initial/equilibrium and stagnant state of the water droplet. For both the initial/equilibrium and stagnant states, droplet profiles are observed to have symmetry along its center-of-mass axis and the value of *H* is almost zero. The initial/equilibrium state is defined as the point of time at which the droplet is at equilibrium and no external force acts on it. The stagnant state is described as the instance at which the droplet is under the influence of the thermophoretic force, but the force is insufficient to overcome the resistance due to friction. The droplet is observed to have spread more in the stagnant state than in its initial condition. Similarly, the droplet profile during the forward and backward movement (figure 13(f)) is observed to have an asymmetrical shape. In the forward motion, when the droplet gains speed towards the cold end, the droplet is found to have a very high advancing angle compared to the initial/equilibrium case, resulting in a positive *H* value (8.45°). The momentarily backward movement of the droplet is due to the large oscillation of thermal fluctuations, although the thermophoretic force drives the droplet forward on average. The droplet oscillates during the process causing a negative *H* value (−12.46°). The instantaneous movement of the contact line under the influence of a thermal gradient is the reason for dynamic contact angle. The water droplet transport was steady and stable in water–*h*-BN system, thus there was a negligible oscillation of the droplet during the transport. The contact angle hysteresis is more pronounced for graphene than for the *h*-BN sheet, hence the results are presented only for the water–graphene system.

The isothermal diffusion coefficient is measured following an equilibrium MD computation which is simulated for 20 ns at 300 K. The moment scaling spectrum (MSS) method is used to measure the translational mobility imposed on the fluid by a thermal gradient [43, 44], where the moments of displacement μ are calculated from the motion of the center-of-mass position

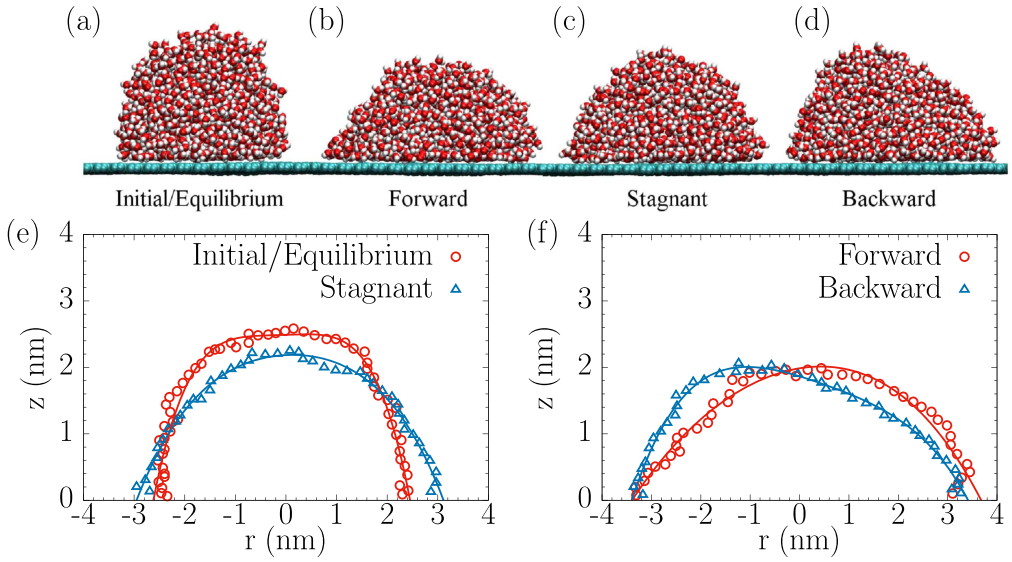

Figure 13. (a)–(d) The dynamic behavior of the water droplet on the graphene surface. (e), (f) The third order polynomial fit is used for extrapolating the isodensity points, to represent the droplet profiles of various dynamic states.

z_{cm} of the water droplet. The moment for a specific frame-shift Δn of order ν can be defined as

$$\mu(\Delta n) = \frac{1}{N - \Delta n} \sum_{n=1}^{N-\Delta n} |z_{cm}(n + \Delta n) - z_{cm}(n)|^{\nu}, \quad (3)$$

where $n = 1, 2, 3, .., N$, with N the total number of trajectory points. The mean-squared displacement, which is commonly used to calculate the classical self-diffusion coefficient of fluids, is a particular case of the MSS of order 2. The moments are calculated up to 6 orders to quantify the diffusion modes of the water droplets. The scaling coefficient γ_{ν} for any order can be determined from the slope of the linear least-squares regression profile of the logarithmic data for the moment of displacements, as discussed in our previous work [14]. The MSS is defined as the direct relationship between the scaling coefficient γ_{ν} and the order ν (figure 14). The slope of the linear profile (S_{MSS}) indicates the type of diffusive motion of the fluid droplet; with slopes of S_{MSS}= 0, 0.5 and 1, representing no diffusive motion, self-similar diffusion (blue dashed line) and ballistic motion (red dashed line), respectively. The region between these diffusive types is represented by various diffusive regimes. The area below the line of the self-similar diffusion is the sub-diffusive regime ($0 < S_{MSS} < 0.5$). The area between the lines of self-similar diffusion and the ballistic motion is the super-diffusive regime ($0.5 < S_{MSS} < 1$). Thus, for a long-time scaling, S_{MSS} for graphene and *h*-BN systems are found to be 0.36 and 0.57, respectively. The slope, S_{MSS} of the water-graphene system lies in the range of the sub-diffusive regime. Whereas, the S_{MSS} of the water–*h*-BN system lies in the range of the super-diffusive regime, which results in a faster fluid transport on the *h*-BN sheet. This result supports the earlier claims made about the energetic and force analysis. The water droplet moves to the energetically favorable location on both surfaces, where the droplet can possess lower potential energy. These findings give insight into the previously unexplored mechanism of a thermophoretic droplet transport on the two-dimensional surfaces.

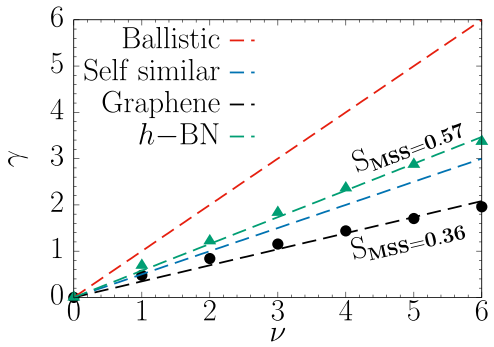

Figure 14. The moment scaling spectrum, the black and green dots indicate the scaling coefficients of the water–graphene and water–*h*-BN systems. The black and green dashed line indicates a linear fit with a slope 0.36 and 0.57 for the graphene and *h*-BN systems respectively. Red and blue dashed lines indicate the ballistic and self-similar diffusion, respectively.

4. Conclusion

Through molecular dynamics simulations, we have demonstrated that a water droplet can be transported across a surface by imposing a thermal gradient along the length of the substrate. A water droplet was thermophoretically transported on a graphene and *h*-BN surface. These surfaces have different wettabilities with a significant effect on the droplet transport. The droplet on the graphene surface oscillates and takes longer to reach the other end than on the *h*-BN surface. Energetic analysis was performed to calculate the thermophoretic forces. For the thermal gradient of 2.5 K nm^{-1}, the graphene and *h*-BN sheets produced an average thermophoretic force of 1.51 and 3.19 pN, respectively, whereas a

water-carbon nanotube system produced 7.13 pN for the same thermal gradient [14]. Contact angle hysteresis is monitored during the droplet transport on the graphene surface, which provided insight into the basics of the contact line movement and droplet deformation during thermophoresis. Since the graphene sheet is more hydrophobic than the *h*-BN surface, fewer molecules are in direct contact with the graphene surface. This has led to lower thermophoretic force and hence the droplet motion is also slower on the graphene surface. The MSS analysis was performed to determine the characteristics of the droplet motion. The droplet showed the attributes of the sub-diffusive process on the graphene surface, while it was super-diffusive on the *h*-BN surface. This study gives a comprehensive approach to nano-droplet transport on a surface, which is necessary to develop novel methods of nano-transportation and nano-heat management systems.

Acknowledgments

We thank the financial support received from the Science and Engineering Research Board (SERB), the Department of Science and Technology (DST) and the Government of India through project number EMR/2016/005396.

ORCID iDs

Sarith P Sathian https://orcid.org/0000-0003-2756-7210

References

[1] Hilal N, Al-Zoubi H, Darwish N A, Mohamma A W and Abu Arabi M 2004 A comprehensive review of nanofiltration membranes: treatment, pretreatment, modelling, and atomic force microscopy *Desalination* **170** 281–308
[2] Hsieh S S, Leu H Y and Liu H H 2015 Spray cooling characteristics of nanofluids for electronic power devices *Nanoscale Res. Lett.* **10** 139
[3] Liu B, Wu R, Baimova J A, Wu H, Law A W K, Dmitriev S V and Zhou K 2016 Molecular dynamics study of pressure-driven water transport through graphene bilayers *Phys. Chem. Chem. Phys.* **18** 1886
[4] Duhr S and Braun D 2006 Why molecules move along a temperature gradient *Proc. Natl Acad. Sci. USA* **103** 19678–82
[5] Dutrieux J F, Platten J K, Chavepeyer G and Bou-Ali M M 2002 On the measurement of positive soret coefficients *J. Phys. Chem.* B **106** 6104–14
[6] Thekkethala J F and Sathian S P 2013 Thermal transpiration through single walled carbon nanotubes and graphene channels *J. Chem. Phys.* **139** 174712
[7] Fedorov A S and Sadreev A F 2009 Thermoactivated transport of molecules H_2 in narrow single-wall carbon nanotubes *Eur. Phys. J.* B **69** 363–8
[8] Zambrano H A, Walther J H, Koumoutsakos P and Sbalzarini I F 2009 Thermophoretic motion of water nanodroplets confined inside carbon nanotubes *Nano Lett.* **9** 66–71
[9] Schoen P A E, Walther J H, Arcidiacono S, Poulikakos D and Koumoutsakos P 2006 Nanoparticle traffic on helical tracks: thermophoretic mass transport through carbon nanotubes *Nano Lett.* **6** 1910–7
[10] Soret C 1881 Sur L'tat D'quilibre Que Prend au Point de Vue de sa Concentration une Dissolution Saline Primitivement Homohne Dont Deux Parties Sont Portes des Tempratures Diffrentes *Ann. Chim. Phys.* **22** 293–7
[11] Guo Z Y, Hou Q W and Cao B Y 2012 A novel thermal driving force for nanodevices *J. Heat Transfer* **134** 51010
[12] William M, John B, Deborah K and Michael R J 2008 Hydrothermal vents and the origin of life *Nat. Rev. Microbiol.* **6** 805–14
[13] Shiomi J and Maruyama S 2009 Water transport inside a single-walled carbon nanotube driven by a temperature gradient *Nanotechnology* **20** 055708
[14] Rajegowda R, Kannam S K, Hartkamp R and Sathian S P 2017 Thermophoretic transport of ionic liquid droplets in carbon nanotubes *Nanotechnology* **28** 155401
[15] Holt J K, Park H G, Wang Y, Stadermann M, Artyukhin A B, Grigoropoulos C P, Noy A and Bakajin O 2006 Fast mass transport through sub-2-nanometer carbon nanotubes *Science* **312** 1034–7
[16] Kolesnikov A I, Zanotti J M, Loong C K, Thiyagarajan P, Moravsky A P, Loutfy R O and Burnham C J 2004 Anomalously soft dynamics of water in a nanotube: a revelation of nanoscale confinement *Phys. Rev. Lett.* **93** 035503
[17] Babu J S and Sathian S P 2011 The role of activation energy and reduced viscosity on the enhancement of water flow through carbon nanotubes *J. Chem. Phys.* **134** 194509
[18] Shiomi J, Han J and Maruyama S 2007 Molecular dynamics of ice-nanotube formation inside carbon nanotubes *J. Phys. Chem.* C **111** 12188–93
[19] Koga K, Gao G T, Tanaka H and Zeng X C 2001 Formation of ordered ice nanotubes inside carbon nanotubes *Nature* **412** 802–5
[20] Wei N, Wang H Q and Zheng J C 2012 Nanoparticle manipulation by thermal gradient *Nanoscale Res. Lett.* **7** 154
[21] Somada H, Hirahara K, Akita S and Nakayama Y 2009 A molecular linear motor consisting of carbon nanotubes *Nano Lett.* **9** 62–5
[22] Guo Z, Chang T, Guo X and Gao H 2012 Mechanics of thermophoretic and thermally induced edge forces in carbon nanotube nanodevices *J. Mech. Phys. Solids* **60** 1676–87
[23] Shenai P M, Xu Z and Zhao Y 2011 Thermal-gradient-induced interaction energy ramp and actuation of relative axial motion in short-sleeved double-walled carbon nanotubes *Nanotechnology* **22** 485702
[24] Rurali R and Hernandez E R 2010 Thermally induced directed motion of fullerene clusters encapsulated in carbon nanotubes *Chem. Phys. Lett.* **497** 62–5
[25] Savin A V and Kivshar Y S 2012 Transport of fullerene molecules along graphene nanoribbons *Sci. Rep.* **2** 1012
[26] Becton M and Wang X 2014 Thermal gradients on graphene to drive nanoflake motion *J. Chem. Theory Comput.* **10** 722–30
[27] Yuan Z, Yongdan Z and Meiya L 2016 Lattice thermal conductivity of boron nitride nanoribbon from molecular dynamics simulation *Wuhan Univ. J. Nat. Sci.* **21** 461–5
[28] Singh S K, Neek-Amal M, Costamagna S and Peeters F M 2013 Thermomechanical properties of a single hexagonal boron nitride sheet *Phys. Rev.* B **87** 184106
[29] Plimpton S 1995 Fast parallel algorithms for short-range molecular dynamics *J. Comput. Phys.* **117** 1–19
[30] Berendsen H J C, Grigera J R and Straatsma T P 1987 The missing term in effective pair potentials *J. Phys. Chem.* **91** 6269–71

[31] Maginn E J 2009 Molecular simulation of ionic liquids: current status and future opportunities *J. Phys.: Condens. Matter* **21** 373101
[32] Brenner D W, Shenderova O A, Harrison J A, Stuart S J, Ni B and Sinnott S B 2002 A second-generation reactive empirical bond order (REBO) potential energy expression for hydrocarbons *J. Phys.: Condens. Matter* **14** 783
[33] Tersoff J 1989 Modeling solid-state chemistry: interatomic potentials for multicomponent systems *Phys. Rev.* B **39** 5566–8
[34] Li H and Zeng X C 2012 Wetting and interfacial properties of water nanodroplets in contact with graphene and monolayer boron-nitride sheets *ACS Nano* **6** 2401–9
[35] Ritos K, Dongari N, Borg M K, Zhang Y and Reese J M 2013 Dynamics of nanoscale droplets on moving surfaces *Langmuir* **29** 6936–43
[36] Li J and Wang F 2017 Water graphene contact surface investigated by pairwise potentials from force-matching PAW-PBE with dispersion correction *J. Chem. Phys.* **146** 054702
[37] Taherian F, Marcon V, Van der Vegt N F A and Leroy F 2013 What is the contact angle of water on graphene? *Langmuir* **29** 1457–65
[38] Giovambattista N, Debenedetti P G and Rossky P J 2007 Effect of surface polarity on water contact angle and interfacial hydration structure *J. Phys. Chem.* B **111** 9581–7
[39] Trudeau T G, Jena K C and Hore D K 2009 Water structure at solid surfaces of varying hydrophobicity *J. Phys. Chem.* C **113** 20002–8
[40] Wu Y, Wagner L K and Aluru N R 2016 Hexagonal boron nitride and water interaction parameters *J. Chem. Phys.* **144** 164118
[41] Vega C, Sanz E and Abascal J L F 2005 The melting temperature of the most common models of water *J. Chem. Phys.* **122** 114507
[42] Falk K, Sedlmeier F, Joly L, Netz R R and Bocquet L 2010 Molecular origin of fast water transport in carbon nanotube membranes: superlubricity versus curvature dependent friction *Nano Lett.* **10** 4067–73
[43] Ferrari R, Manfroi A J and Young W R 2001 Strongly and weakly self-similar diffusion *Physica* D **154** 111–37
[44] Sbalzarini I F and Koumoutsakos P 2005 Feature point tracking and trajectory analysis for video imaging in cell biology *J. Struct. Biol.* **151** 182–95